Dynamics of Atmospheres and Oceans 113 (2026) 101642

Contents lists available at ScienceDirect

Dynamics of Atmospheres and Oceans

journal homepage: www.elsevier.com/locate/dynatmoce

Impact of ENSO on the genesis potential index of cyclones over the Bay of Bengal during the post-monsoon season

P. Suneeta [a,*], TVS Udaya Bhaskar [a], S.S.V.S. Ramakrishna [b]

[a] Ocean Data Management Group, Indian National Centre for Ocean Information Services (INCOIS), Ministry of Earth Sciences (MoES), Govt. of India, Hyderabad, India

[b] Department of Meteorology and Oceanography, College of Science and Technology, Andhra University, Visakhapatnam, India

ARTICLE INFO

Keywords:
Tropical cyclone
Genesis Potential Index
El-Niño-Southern Oscillation
Upper Ocean Heat Content
Sea surface Height Anomaly

ABSTRACT

Tropical Cyclones (TCs) are among the most destructive weather phenomena, causing substantial damage to coastal regions and vulnerable communities along the Bay of Bengal. Predicting their formation remains a significant challenge due to the complex interactions between atmospheric and oceanic processes. This study investigates the influence of the El Niño–Southern Oscillation (ENSO) on the Genesis Potential Index (GPI) and the Total Number of Depressions and Cyclones (TNDC) over the Bay of Bengal (5°–20°N, 80°–100°E) during the post-monsoon season (October–December) from 1995 to 2019. Cyclone activity associated with El Niño, La Niña, and Neutral ENSO phases is examined using four GPI formulations based on key atmospheric and oceanic parameters, including a newly developed index from our previous research. The results reveal pronounced ENSO-dependent variations in vertical wind shear, Upper Ocean Heat Content (UOHC), depth of the 26 °C isotherm (D26), Sea Surface Temperature (SST), Sea Surface Height Anomaly (SSHA), latent heat flux, net longwave radiation, and low-level relative vorticity. During La Niña years, reduced vertical wind shear, enhanced low-level cyclonic vorticity, deeper thermocline, higher UOHC, and increased air–sea heat fluxes create a dynamically and thermodynamically favorable environment for cyclone genesis, leading to GPI values nearly twice those observed during El Niño and Neutral phases. These findings demonstrate the critical role of ENSO-driven atmospheric–oceanic coupling in modulating cyclone genesis over the Bay of Bengal and highlight the importance of incorporating ENSO-related variability into regional cyclone forecasting and disaster risk management strategies.

1. Introduction

Understanding the influence of large-scale environmental conditions on tropical cyclogenesis is imperative from scientific and socioeconomic perspectives. The Bay of Bengal, particularly its southern region, serves as a primary genesis zone for a significant portion of cyclones during the post-monsoon season (October-December). Generally, these TCs exhibit a westward or north-westward trajectory before making landfall along the eastern coast of India. Some TCs deviate northward or northeastward, impacting the shores of Bangladesh and Myanmar (Sadhuram et al., 2004, 2006). Previous studies have extensively examined the functional and structural characteristics of TC vortices during intensification, highlighting symmetric features such as mesovortices, convective hot towers or

* Corresponding author.
E-mail address: ponnagantisuneeta@gmail.com (P. Suneeta).

https://doi.org/10.1016/j.dynatmoce.2025.101642
Received 19 May 2025; Received in revised form 22 December 2025; Accepted 30 December 2025
Available online 2 January 2026

bursts, and outflow jets (Emanuel, Noolan, 2004). Vertical wind shear, a critical factor impeding cyclone development, is commonly assessed by comparing wind speed and direction at 850 and 200 mb geopotential heights (Yaukey, 2014). In the North Indian Ocean, most TCs undergo formation and intensification during April and May (pre-monsoon season) and October and November (post--monsoon season). This temporal pattern underscores the significance of understanding this regions dynamics and environmental drivers governing cyclone genesis and intensification. Many previous studies have advanced our understanding of the relationship between ENSO and TCs across different ocean basins. Early studies by Royer et al. (1998), Roy Bhowmik (2003) and While the Emanuel, Noolan (2004) GPI, which includes MPI, is a widely used metric, the present study focuses on GPIZ1 and GPIS, which incorporate oceanic parameters relevant to the Bay of Bengal post-monsoon season. Inclusion of MPI-based GPI will be considered in future work to further assess its complementarity with the present indices. Wu et al. (2004) and Camargo et al. (2007) analyzed ENSO's influence on cyclone frequency and intensity, while DeMaria et al. (2001) introduced a genesis parameter for assessing cyclone formation probability in the Atlantic region. Yumoto et al. (2001), Camargo, Sobel (2005), and Wada and Usui (2007) highlighted disparities in cyclone characteristics across ENSO phases, and Lin et al. (2021) identified low-level absolute vorticity and mid-level relative humidity as key factors influencing cyclone occurrence. Focusing on the Bay of Bengal, Girishkumar and Ravichandran (2012) demonstrated that ENSO significantly affects cyclone frequency, genesis location, and intensity during the post-monsoon season, with notable shifts in genesis sites under different ENSO phases. Despite these contributions, several gaps remain in understanding the detailed mechanisms through which ENSO modulates cyclone activity over the Bay of Bengal, motivating the present study. In addition to ENSO, several other large-scale climate factors can modulate cyclone activity over the Bay of Bengal. Previous studies have shown that the Indian Ocean Dipole (IOD) influences cyclone genesis by modifying regional sea surface temperature gradients and atmospheric circulation patterns (Du et al., 2011). Arctic sea ice anomalies can also impact cyclone frequency in the following season through teleconnections that alter large-scale atmospheric circulation and convection (Chen et al., 2023). Similarly, SST anomalies in the northern tropical Atlantic have been found to affect tropical cyclogenesis over the western North Pacific by influencing inter-basin circulation and vorticity patterns (Cao et al., 2016). Furthermore, regional Hadley circulation variations over the western Pacific can modulate cyclone activity through changes in vertical motion and shear (Huang et al., 2024). Although our study primarily focuses on ENSO, these additional climate drivers may interact with ENSO phases, further modulating GPI and cyclone activity in the Bay of Bengal. A detailed assessment of these factors could be considered in future studies to provide a more comprehensive understanding of cyclone genesis in this region. Many studies have focused on only one or two parameters; however, the present study examines atmospheric and oceanic parameters, providing more accurate relationships and insights.

Several studies have examined the relationship between ENSO and cyclone activity over the North Indian Ocean (NIO), particularly the Bay of Bengal (BoB). Chan et al., Chia and Ropelewski (2002), and Ta-Huu and Sato (2018) demonstrated that ENSO modulates cyclone frequency, genesis location, and intensity in this region. Additional studies have reported ENSO-related variations in cyclone activity through changes in large-scale circulation, vertical wind shear, and thermodynamic conditions (Singh et al., 2000; Goswami et al., 2003; Sadhuram et al., 2012; Vissa et al., 2013; Mahala et al., 2015). Felton et al. (2013) further highlighted ENSO's significant influence on post-monsoon cyclone activity over the Bay of Bengal, although the underlying mechanisms remain uncertain. Observational and modeling studies have shown that ENSO modulates cyclone genesis potential by influencing coupled atmospheric–oceanic processes (Tippet et al., 2011; Bruyère et al., 2012; Liu and Chan, 2013; Harla et al., 2013; Mishra et al., 2019; Brian et al., 2020). Building on this framework, Zhang et al. (2016) introduced a Genesis Potential Parameter incorporating both atmospheric and oceanic factors, while Suneeta and Sadhuram (2018) and Suneeta and Ramakrishna (2021) emphasized the critical role of oceanic parameters in cyclone genesis and intensification over the NIO (Lin and Chan, 2015; Hu et al., 2018; Xu et al., 2020).

Despite these advances, the combined effects of atmospheric and oceanic parameters on cyclone genesis under varying ENSO phases over the Bay of Bengal remain insufficiently understood. To address this gap, the present study investigates the impact of ENSO on the Genesis Potential Indices (GPIs) and the TNDC during the post-monsoon season (October–December) for the period 1995–2019. By employing four different GPI formulations, including one developed in our previous work, this study aims to provide a comprehensive understanding of the relative importance of key atmospheric and oceanic factors influencing cyclone genesis and intensification in the Bay of Bengal. Previous studies have developed several Genesis Potential Indices (GPIs) to quantify the likelihood of cyclone formation using atmospheric and oceanic parameters. For instance, Kotal et al. (2009) proposed a GPI formulation emphasizing the role of relative vorticity, thermal instability, and vertical wind shear over the North Indian Ocean, while Zhang et al. (2016) integrated oceanic parameters such as the 26°C isotherm depth and heat fluxes to improve cyclone prediction over the northwestern Pacific. Similarly, Suneeta and Sadhuram (2018) introduced a modified GPI that incorporates Upper Ocean Heat Content (UOHC), Sea Surface Height Anomaly (SSHA), and Sea Surface Temperature (SST), highlighting the influence of oceanic conditions on cyclone genesis. These studies collectively underscore the importance of combining atmospheric and oceanic variables to better understand the mechanisms governing cyclone formation.

Felton et al. (2013) examined the ENSO - Cyclone relationship over the Bay of Bengal and provided detailed insights into the mechanisms through which ENSO modulates post-monsoon cyclone activity in this region. However, despite the progress made in these studies, a comprehensive understanding of how ENSO influences the spatial distribution and intensity of cyclone genesis potential across different environmental parameters in the Bay of Bengal remains limited.

To address this gap, the present study investigates the spatial variability of multiple GPIs and their association with TNDC during different ENSO phases El Niño, La Niña, and Neutral years over the Bay of Bengal. By integrating both atmospheric and oceanic parameters, this research aims to provide an improved understanding of the environmental controls on cyclone genesis during the post-monsoon season. The study seeks to clarify how variations in key parameters such as relative vorticity, vertical wind shear, SST, and upper ocean heat content contribute to changes in cyclone activity under varying ENSO conditions. The findings are expected to enhance the understanding of regional cyclone climatology and support more accurate prediction and mitigation strategies for coastal

vulnerability in the Bay of Bengal region.

2. Data and methodology

The present study investigates the influence of oceanic and atmospheric parameters on cyclone genesis during different ENSO phases over the BoB for the post-monsoon season (October–December). The GPI formulations were derived from both dynamic and thermodynamic parameters to understand the variability of cyclone genesis during El Niño, La Niña, and Neutral conditions. This study employed four distinct GPIs. The first GPI, referred to as GPIK, follows the methodology outlined by Kotal et al. (2009). This approach aligns with the GPI currently utilized by the India Meteorological Department (IMD). The GPIK is computed using the following equation:

$$\mathbf{GPIK} = \frac{\boldsymbol{\xi_{850}} \times \boldsymbol{M} \times \boldsymbol{I}}{\boldsymbol{S}} \mathbf{if} \boldsymbol{\xi_{850}} > \boldsymbol{0}, \boldsymbol{M} > \boldsymbol{0} \mathbf{and} \boldsymbol{I} > \boldsymbol{0} \rightarrow$$

$$= \boldsymbol{0} \mathbf{if} \boldsymbol{\xi_{850}} \leq \boldsymbol{0}, \boldsymbol{M} \leq \boldsymbol{0} \mathbf{or} \boldsymbol{I} \leq \boldsymbol{0} \quad (1)$$

Where

ξ_{850} =low -level relative vorticity (at 850 hPa) in 10^{-5} S^{-1};

S= vertical wind shear between 200 hPa and 850 hPa (m S^{-1});

$M = \frac{[RH-40]}{30}$ = Middle troposphere relative humidity;

Where RH is the average relative humidity between 700 hPa and 500 hPa;

I = (T850-T500)^{0}C = middle tropospheric instability (Temperature difference between 850 hPa and 500 hPa).

For the western North Pacific Ocean, Zhang et al. (2016) developed an equation. In this analysis, GPI as given in Eqs. 2 and 3 are utilized. These are denoted as GPIZ1 and GPIZ2, respectively.

$$\mathrm{GPIZ1} = p|10^5\eta_{1000}|^{0.9}\left(\frac{\overline{T}}{26}\right)^{7.64}\left(\frac{F}{45}\right)^{-2.73}\left(\frac{D_{26}}{80}\right)^{0.25} \quad (2)$$

Where η is the absolute vorticity at 1000 hPa, $\overline{T}$ is the average sea water temperature, F is the net long wave radiation (W/m2), and D26 is the depth of the 26 °C isotherm. The coefficient p allows for the best least square fit between GPI ocean and observations with $p = 7.4 \times 10^{-3}$.

$$\mathrm{GPIZ2} = p|10^5\eta_{850}|^{1.2}\left(\frac{(-\omega + 0.1)}{0.1}\right)^{1.8}\left(\frac{LH}{100}\right)^{-0.6}\left(\frac{\overline{T}}{26}\right)^{10}\left(\frac{D_{26}}{80}\right)^{0.13} \quad (3)$$

Where η is absolute vorticity at 850 hPa; ω is the vertical velocity at 500 hPa, LH denotes the latent heat flux with $p = 1.5 \times 10^{-2}$.

Atmospheric variables such as relative vorticity, relative humidity, vertical velocity (Ω), and temperature were obtained from the ERA5 reanalysis dataset provided by the European Centre for Medium-Range Weather Forecasts (ECMWF) at a spatial resolution of $0.25^\circ \times 0.25^\circ$.

Monthly averaged SST, Thermal instability (I) and vertical wind shear (S) were derived from ERA5 data. Thermal instability was calculated as the temperature difference between 850 hPa and 500 hPa levels (T850 − T500), while vertical wind shear was computed from the horizontal wind components at 850 hPa and 200 hPa levels. ERA5 offers high-resolution global data at $0.25^\circ \times 0.25^\circ$ spatial resolution with hourly estimates on 137 vertical levels from 1950 to the present (available at https://cds.climate.copernicus.eu/datasets/reanalysis-era5-pressure-levels).

Following the formulation of the GPI proposed by Kotal et al. (2009), an extended version incorporating oceanic parameters was introduced by Suneeta and Sadhuram (2018), referred to as the Genesis Potential Index with Oceanic Influence (GPIS). The GPIS is expressed as:

$$\mathbf{GPIS} = \mathbf{GPIK}^* \left(\frac{\boldsymbol{UOHC}}{\boldsymbol{40}}\right) \quad (4)$$

The upper ocean heat content (UOHC) is calculated using the multiple regression equation proposed by Ali et al. (2012)

$$\mathbf{UOHC} = \mathbf{-245.256} + \mathbf{D26}^*\mathbf{0.982} + \mathbf{SSHA}^*\mathbf{1.243} + \mathbf{SST}^*\mathbf{8.417} \quad (4.1)$$

In this study, UOHC was estimated using the multiple regression formulation proposed by Ali et al. (2012), which provides reliable estimates based on satellite-derived surface parameters. A comparison with the Suneeta and Sadhuram (2018) formulation indicated that the difference in estimated UOHC values is within ±5–8 kJ/cm^2 over the Bay of Bengal. Previous studies (Suneeta and Sadhuram, 2018; Suneeta and Ramakrishna, 2021) have also shown that the Ali et al. (2012) equation exhibits a better correlation with in situ observations. Therefore, this approach was adopted for the present analysis to ensure consistency with reanalysis data and long-term variability studies.

$$\mathbf{D26} = \mathbf{63.84} + \mathbf{1.39}^*\mathbf{SSHA} + \mathbf{0.044SSHA}^*\mathbf{SSHA} \quad (4.2)$$

(Eq. 4.2 from Sadhuram et al. (2006)).

The estimated D26 from SSHA shows a strong correlation (r = 0.76) with measurements, indicating that SSHA is a reliable proxy. SSHA data (m) were obtained from AVISO Copernicus Marine Services (CMEMS), which provides gridded data at 0.25° × 0.25° resolution.

It is important to note that, unlike earlier studies using coarse-resolution (2.5° × 2.5°) data from IRI/LDEO, this study employed high-resolution ERA-5 and CMEMS datasets to improve accuracy and consistency. A comprehensive dataset spanning 1995–2019 was utilized to analyze ENSO variability, covering several El Niño, La Niña, and Neutral years. In addition, tropical cyclone track and intensity data for the Bay of Bengal were obtained from the India Meteorological Department (IMD) Best Track Dataset (https://rsmcnewdelhi.imd.gov.in/), which provides reliable records of depressions and cyclonic storms over the North Indian Ocean, including genesis location, duration, and intensity. To categorize the years into El Niño, La Niña, and Neutral phases, the Oceanic Niño Index (ONI) provided by the NOAA Climate Prediction Center (https://www.cpc.ncep.noaa.gov/) was used. ONI is defined as the 3-month running mean of sea surface temperature anomalies in the Niño 3.4 region (5°N-5°S, 170°–120°W). Years were classified as El Niño when the ONI ≥ +0.5 °C for at least five consecutive overlapping 3-month seasons, La Niña when the ONI ≤ -0.5 °C for the same duration, and Neutral when the ONI remains between −0.5 °C and + 0.5 °C. This classification allows consistent identification of ENSO phases and facilitates the computation of average composites of environmental parameters and GPIs over the Bay of Bengal during the post-monsoon season (October-December) during which most tropical cyclone formations occur over the BoB. For each ENSO phase, the average values of all parameters during October-December were calculated to derive GPI composites (GPIK, GPIZ1, GPIZ2, GPIS). The spatial distribution of these composites was analyzed to identify key environmental factors influencing cyclone genesis over the BoB.

3. Results and discussion

3.1. Relationship between the ENSO and GPIK

Li et al. (2013) emphasized that both atmospheric and oceanic conditions play a crucial role in modulating tropical cyclone activity over the Bay of Bengal. Based on the average spatial distributions of all GPIs and their corresponding genesis locations during the post-monsoon season, the variations in GPI and the TNDC across the Bay of Bengal were analysed for different ENSO phases. During the study period, a total of 65 TCs formed over the Bay of Bengal, including 33 during La Niña events, 15 during El Niño events, and 17 during Neutral conditions (Table 1). The Total Number of Depressions and Cyclones (TNDC) that developed over the Bay of Bengal during the post-monsoon season under different ENSO phases was analyzed (Table 1). During El Niño years, the number of TCs is relatively lower, with an average of 1.67 TCs per year. La Niña years exhibit a significant increase in cyclone activity, with an average of 3.00 TCs per year. In Neutral years, when ENSO conditions are neither El Niño nor La Niña, the average number of cyclone is 3.40 per year. This indicates moderate cyclone activity falling between the El-Niño and La-Niña years. These findings strongly underscore the influence of ENSO variability on cyclone genesis within the Bay of Bengal region. However, a notable shift in cyclone activity dynamics is observed when only developing depressions (i.e., cyclones with maximum speeds of 35 kt) are considered. From the results obtained from the spatial distributions of GPIK (Eq. 1), it is observed that the relative vorticity ranges between 0 and 5×10^{-6} sec^{-1} during the ENSO period, as depicted in Fig. 1(a-c). Precisely, during the El-Niño period, this range shifts slightly upward to 0–6×10^{-6}, as illustrated in Fig. 1(a), with minimal variation during the La-Niña period. Conversely, the Neutral period extends between 0 and 8×10^{-6}, as shown in Fig. 1(b) and 1 (c), respectively. The relative humidity, as depicted in Fig. 2(a-c), remains within the range of 20–80 % throughout the El-Niño, La-Niña and Neutral periods. Thermal instabilities ranging from 20 to 24°C are illustrated in Fig. 3 (a-c). Vertical wind shear, ranging from 0 to 25 m/sec, is illustrated in Fig. 4(a-c). During the El-Niño period wind shear fluctuates between 0 and 20 m/sec, while during the Neutral period, it varies between 0 and 25 m/sec. Notably, higher wind shear values are observed during specific periods as depicted in Fig. 4(a & c). However, wind shear ranging between 0 and 12 m/sec was observed during the La-Niña period. This indicates that lower-level vertical wind shear values are observed, presenting favorable conditions for the genesis of TCs as shown in Fig. 4(b). The GPIK ranges from 0 to 30×10^{-6} as Fig. 5(a-c) illustrates. TNDC in Table 2 represents the average number of TCs that formed during the post-monsoon season (October to December) across the El-Niño, La-Niña and Neutral phases of ENSO. This was determined by analyzing cyclone track data from the study period (1993–2019) and averaging the number of TCs for each ENSO phase. The values for parameters such as relative vorticity, relative humidity, thermal instability, wind shear and GPIK in Table 2 represent composite averages for each phase derived from ERA5 reanalysis data by averaging the respective values over the corresponding time periods. The results indicate that La-Niña phases show the highest average number of TCs (4.5) coinciding with higher GPIK values and more favorable atmospheric conditions, whereas El-Niño phases exhibit the lowest TNDC (3.3) and

Table 1
Variability of the Total Number of Depressions and Cyclones (TNDC) during the post-monsoon season (October–December) over the Bay of Bengal during El Niño, La Niña, and Neutral composite years.

(ENSO) cycle	(No. of Years)	(No. of Tropical Cyclones)	(Tropical cyclones per year)
El-Niño	09	15	1.67
La-Niña	11	33	3.00
Neutral	05	17	3.40

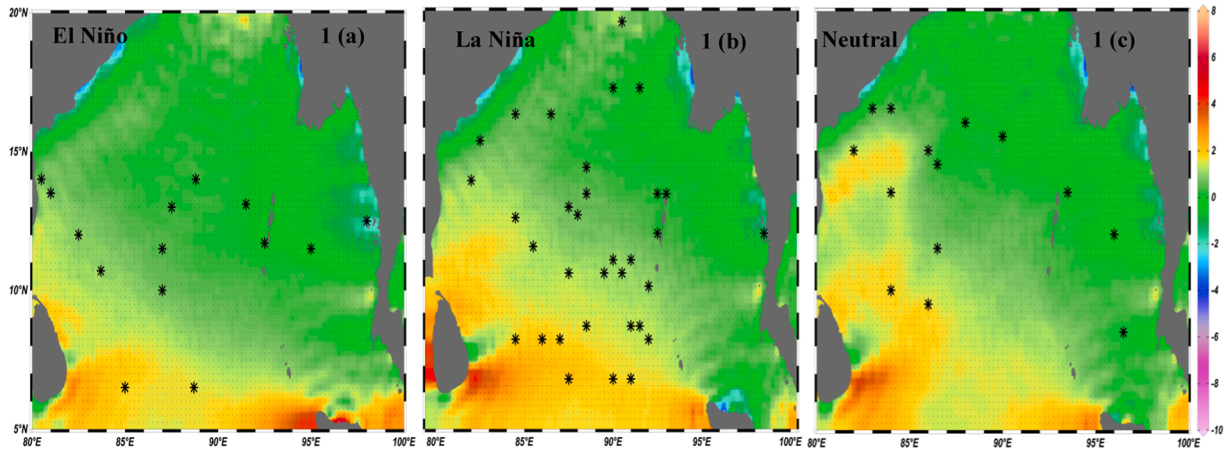

Fig. 1. (a-c): Spatial distribution of Relative Vorticity (RV) during Post monsoon season (October-December) under (a) El Niño (b) La Niña and (c) Neutral years. Black stars indicate the genesis locations.

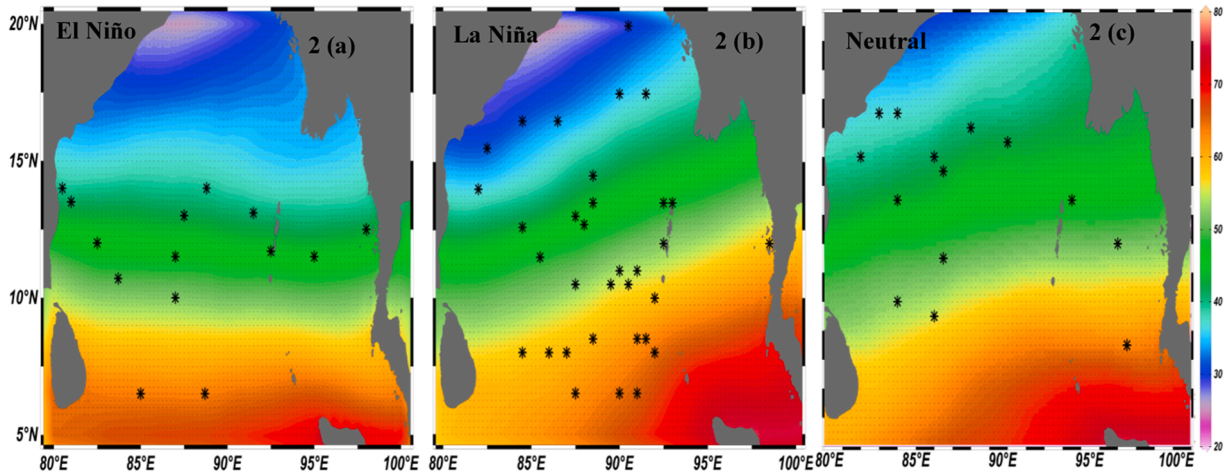

Fig. 2. (a-c): Average relative humidity (%) in the middle troposphere (700–500 hPa) during the post- monsoon season (October–December) for (a) El Niño, (b) La Niña, and (c) Neutral conditions. Black stars denote cyclone genesis points.

reflecting less favorable conditions. The GPIK values presented in Table 2, as well as the GPIs in Tables 3–5 were calculated using the methodology outlined in the manuscript, which integrates atmospheric and oceanic parameters to estimate the genesis potential index. Revealing that all parameters exhibit a stronger correlation with the TNDC formed during the La-Niña period compared to the El-Niño and Neutral periods. Although the spatial composites in Fig. 4 show that the basin-wide vertical wind shear (200–850 hPa) appears slightly lower during El Niño years compared to La Niña, the regional distribution reveals that the zones of reduced shear during El Niño are mostly confined to the southeastern Bay and do not overlap with the main cyclogenesis regions. In contrast, during La Niña years, weaker shear values (around 3–5 m s^{-1}) prevail directly over the central and northern Bay of Bengal, coinciding with areas of enhanced low-level vorticity and moisture. This spatial alignment between low shear, high humidity, and positive vorticity provides a more favorable dynamic environment for tropical cyclone formation. The lower shear values reported in Table 2 correspond to averages calculated specifically over the primary genesis region (10°–20° N, 80°–95° E), which explains their smaller magnitudes compared to the broader range (0–25 m s^{-1}) shown in Fig. 4.

Based on the results, it is concluded that the La Niña period exhibits a strong relationship with both the GPI and TNDC, indicating favourable conditions for the genesis and development of TCs. As shown in Table 2, the thermal stability is lower during La Niña years compared to El Niño years, reflecting enhanced convective activity. Moreover, there is an increase in relative vorticity, relative humidity, and GPIK during La Niña periods, while vertical wind shear remains relatively low (Fig. 4b). The spatial distribution analysis further reveals that the genesis locations of cyclonic disturbances, marked by black stars, are predominantly concentrated in the central Bay of Bengal. Overall, the higher values of vorticity, humidity, and GPIK along with reduced thermal stability and weaker shear during La Niña conditions reaffirm that La Niña phases provide more favourable environmental conditions for both the formation and intensification of cyclonic disturbances. The apparent contradiction arises from differences between basin-wide and genesis-region

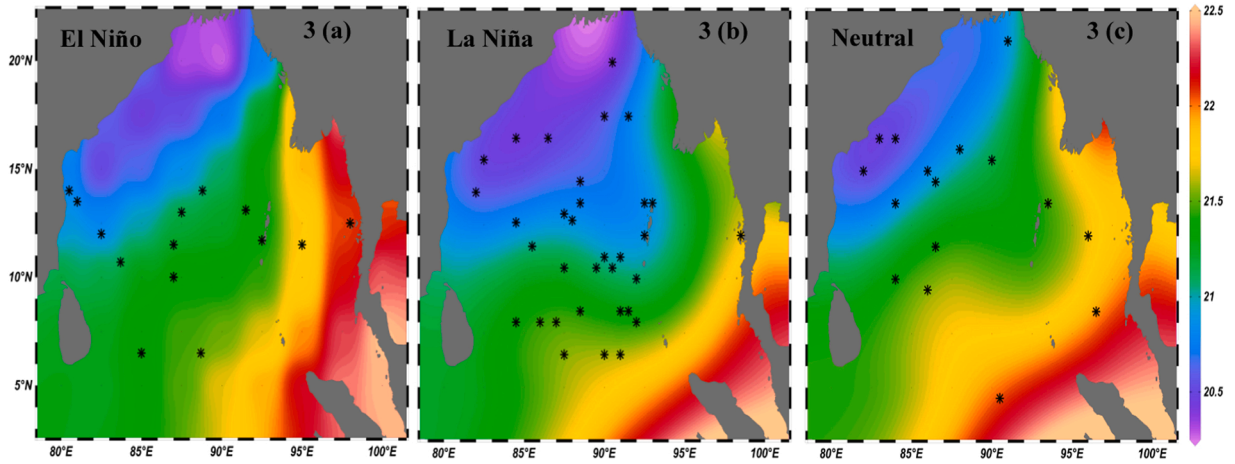

Fig. 3. (a-c): Thermal Instability (TI) middle tropospheric instability (Temperature difference between 850 hPa and 500 hPa for **(a) El Niño, (b) La Niña, and (c) Neutral** conditions.

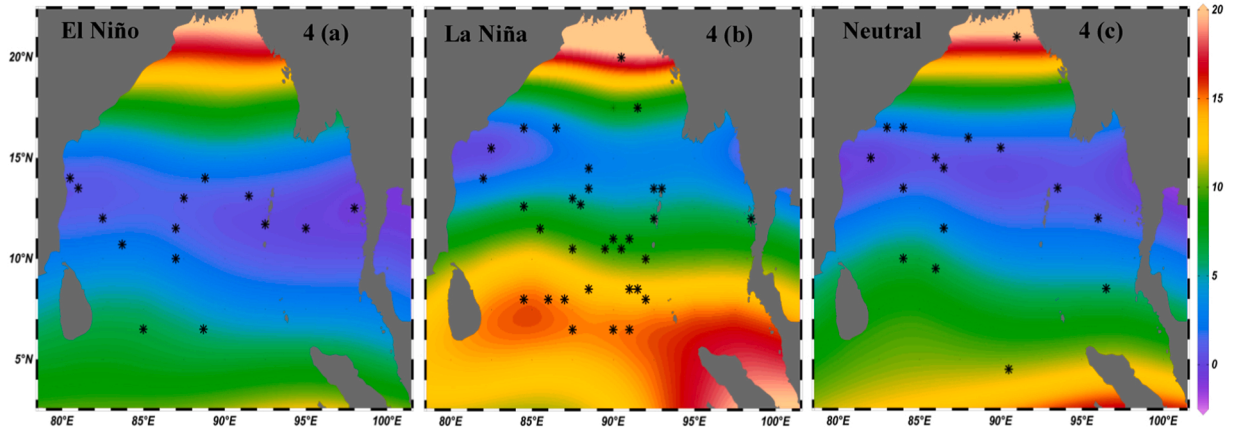

Fig. 4. (a-c): Vertical Wind Shear (WS) between 200 hPa and 850 hPa for **(a) El Niño, (b) La Niña, and (c) Neutral** conditions.

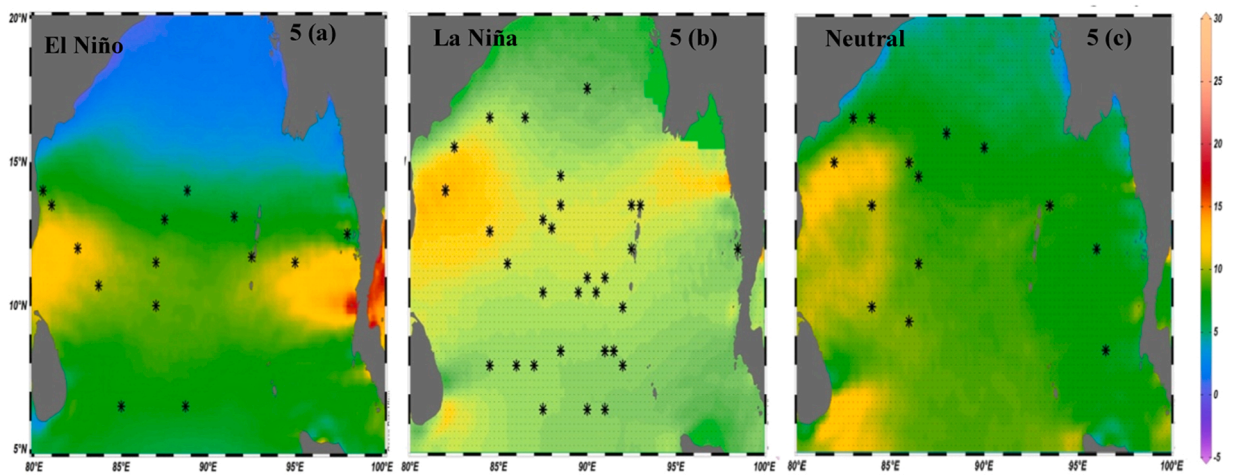

Fig. 5. (a–c): Spatial distribution of the Genesis Potential Index (GPIK) computed using all atmospheric parameters **(a) El Niño, (b) La Niña, and (c) Neutral** conditions.

Table 2
Average composites of Input parameters and GPIK over the Bay of Bengal (BOB) during the Post-monsoon season under El-Niño, La-Niña and Neutral.

Parameter	El-Niño	La-Niña	Neutral
Relative Vorticity ($\times 10^{-5}$ s^{-1}) at 850 hPa	0.1	2.39	1.49
Relative Humidity (averaged between 700 and 500 hPa) (%)	46.83	51.25	50.9
Thermal Instability temperature difference ($T_{850} - T_{500}$) (°C)	21.6	21.35	21.48
Vertical Wind Shear 200 hPa and 850 hPa **(m/s^{-1})**	4.8	3.3	4.89
GPIK	0.76	4.16	2.38
No. of Depressions	5	8	7
No. of Cyclones	10	25	10
TNDC	15	33	17

averages. Table 2 reports shear averaged over the primary genesis zone (10°–20°N, 80°–95°E), where La Niña composites exhibit lower mean 200–850 hPa shear (~3–5 m s^{-1}) than El Niño composites (~4–5 m s^{-1}). Although Fig. 4 shows regions of elevated shear elsewhere in the basin during La Niña, these high-shear areas do not spatially coincide with the vorticity and humidity maxima that define the genesis locations. Therefore, the alignment of low shear with enhanced vorticity and moisture during La Niña provides the dynamically favourable conditions that lead to the higher TNDC observed in Table 2. The intercomparison of mean values of the GPI components between El Niño and La Niña years (Table 2) shows notable differences. Specifically, parameters such as mid-tropospheric relative humidity and potential intensity exhibit statistically significant variations ($p < 0.05$), suggesting their dominant role in modulating cyclonic disturbances during ENSO phases. In contrast, vertical wind shear and vorticity show comparatively weaker or non-significant differences between the two phases, implying that their influence remains relatively stable across ENSO conditions.

3.2. Relationship between the ENSO and GPIZ1

In exploring the relationship between the ENSO and GPIZ1, the average spatial distribution method was employed, as given by Eq. (2). This method incorporates parameters such as D26, SST, F and absolute vorticity (at 1000hPa) as Zhang et al. (2016) outlined. Observations indicate minimal variation in absolute vorticity, ranging from 0 to 15 (x $10^{-5}$$sec^{-1}$), as illustrated in Fig. 6(a-c). SST varies between 26 and 30°C throughout the period with higher values concentrated over the central and Northern parts of the Bay of Bengal during the La-Niña years, as illustrated in Fig. 7(b). Net longwave radiation (F) ranges from 50 to 75 w/m2 across the study period, depicted in Fig. 8(a-c) while D26 varies between 50 and 110 m with the highest value observed during La-Niña and Neutral periods as depicted in Fig. 9(b) and 9 (c) respectively. GPIZ1 computed from Eq. (2) ranges from 0 to 10 (x 10^{-2}) with the highest values observed during La-Niña years as illustrated in Fig. 10 (a-c). However, a comparative analysis of El-Niño, La-Niña and Neutral

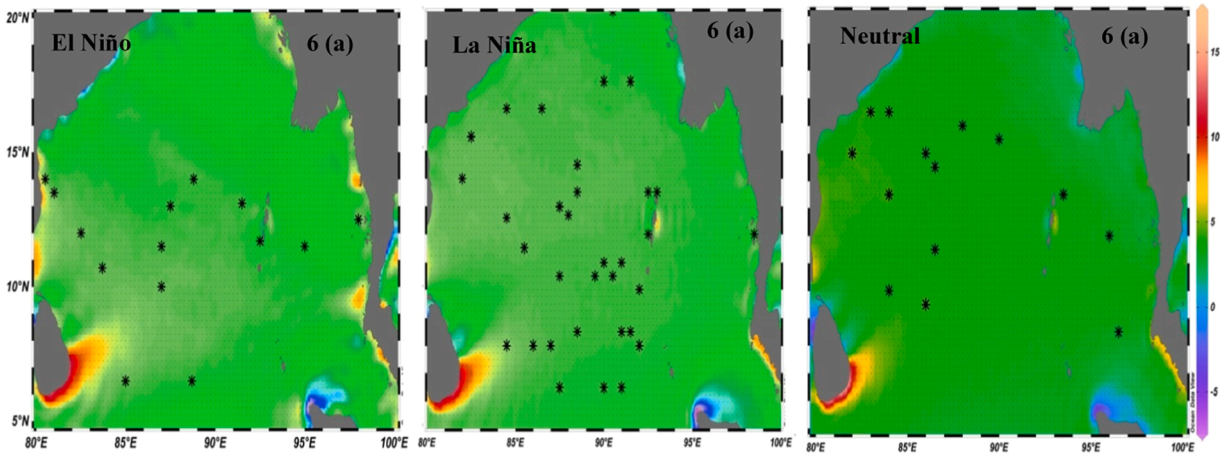

Fig. 6. (a-c): Spatial distribution of absolute vorticity at 1000 hpa during post monsoon season (October-December) under (a) El Niño (b) La Niña and (c) Neutral years. Black stars indicates the genesis locations.

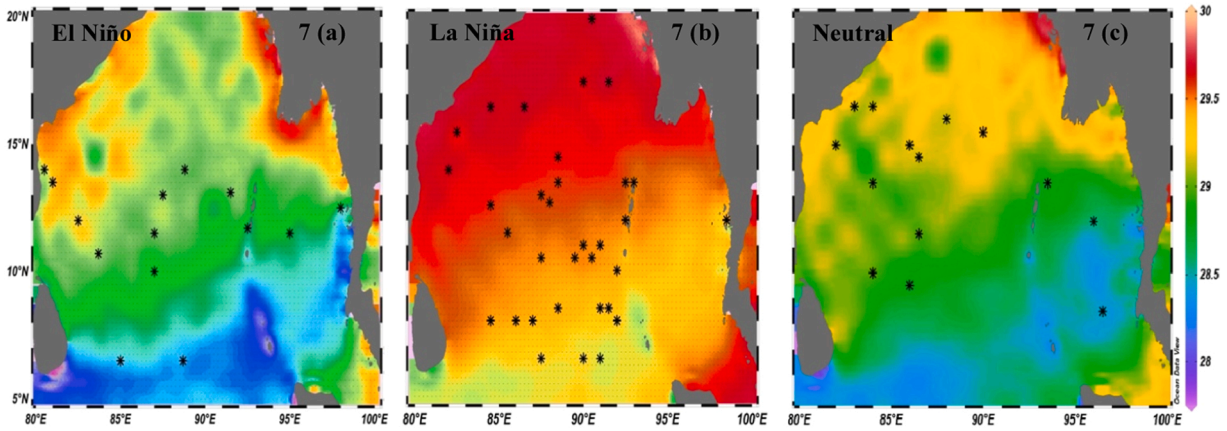

Fig. 7. (a-c): Average Sea Water Temperature ($\overline{T}$) under (a) El Niño (b) La Niña and (c) Neutral years. Black stars indicates the genesis locations.

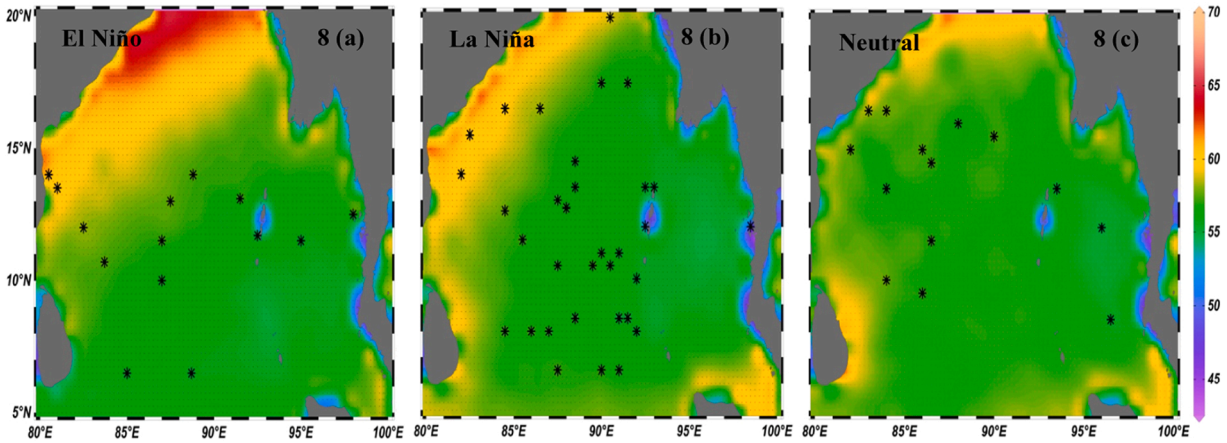

Fig. 8. (a-c): Net long wave radiation (F) under (a) El Niño (b) La Niña and (c) Neutral years. Black stars indicate the genesis locations.

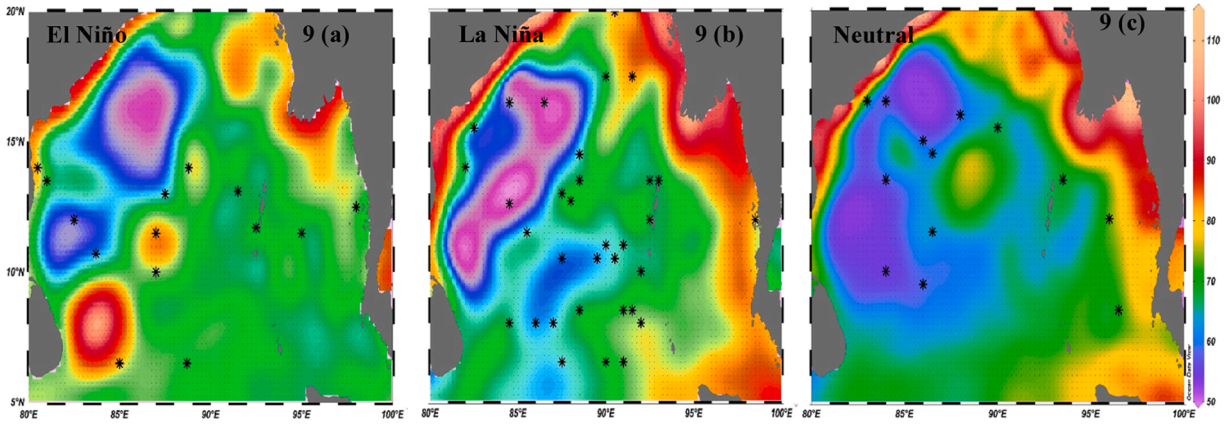

Fig. 9. (a-c): D26 (depth of 26 °C isotherm) under (a) El Niño (b) La Niña and (c) Neutral years. Black stars indicate the genesis locations.

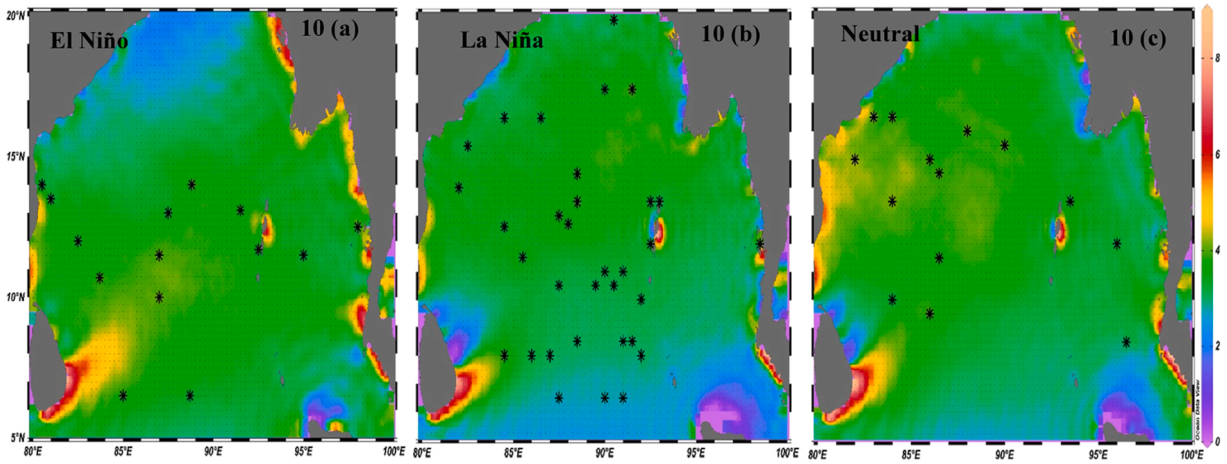

Fig. 10. (a-c): Spatial distribution of the Genesis Potential Index (GPIZ1) under **(a) El Niño, (b) La Niña, and (c) Neutral** conditions.

Table 3
Average composites of Input parameters and GPIZ1 over the Bay of Bengal (BOB) during the Post-monsoon season under El-Niño, La-Niña and Neutral period.

Parameter	El-Niño	La-Niña	Neutral
η 1000 (sec^{-1})	2.82	2.91	2.56
SST (° C)	28.57	28.77	28.49
F (w/m^2)	55.5	54.2	55
D_{26} (m)	66.1	70.27	68
GPIZ1	3.3	3.5	3.2
TNDC	3.3	4.5	3.8

years suggests that La-Niña years are more conducive to the development of cyclone. This inference is further supported by the findings from average composites where all parameters except 'F' exhibit higher values, as presented in Table 3. The observed increase in SST and D26 during the La-Niña periods underscores their significance in the genesis and intensification of cyclonic disturbances, as indicated by GPIZ1. Higher SSTs and a slightly deeper D26 during La Niña years indicates a thicker warm upper ocean layer, which can supply additional oceanic heat content to developing cyclones. This enhanced heat reservoir may support cyclone genesis and intensification, even when atmospheric parameters show only marginal variations contribute to higher GPI values indicating an increased likelihood of cyclone genesis. However, it's essential to note that La-Niña conditions favour cyclone development. Most of the environmental parameters (η 1000, SST, F, D26, GPIZ1) show only marginal differences between ENSO phases, indicating similar large-scale conditions over the Bay of Bengal during the post-monsoon season. Nevertheless, TNDC exhibits a noticeable increase during La Niña years, implying that subtle changes in environmental conditions, possibly along with other dynamical processes, may enhance cyclone genesis during these years.

3.3. Relationship between the ENSO and GPIZ2

Eq. 3, developed by Zhang et al. (2016) and referred to as GPI by including atmosphere and ocean parameters, is indicated as GPIZ2. The first term of GPIZ2 is absolute vorticity at 850 hPa, which exhibits a range of 0–15 (X 10^{-5}), as illustrated in Fig. 11 (a-c). The highest values are observed during La-Niña and Neutral years, as depicted in Fig. 11 (b-c). The second term, representing vertical velocity at 500 hPa, ranges from 3 to 0.5 (x 10^{-2} pa.sec-1), as shown in Fig. 12 (a-c).

Throughout the study period, latent heat flux remains consistently greater than 60 w/m^2 as illustrated in Fig. 13 (a-c), with the highest value of 160 w/m^2 observed during La-Niña and Neutral years. More cyclonic disturbances formed in the Bay of Bengal during the La-Niña period, as depicted in Fig. 13 (b), compared to the Neutral period. Notably, the values of D26 and SST remain consistent for both GPIZ1 and GPIZ2 from Eqs. 2 and 3. GPIZ2 exhibits a range of 0–80 (x 10^{-1}), as shown in Fig. 14 (a-c). The average composites suggest an upward trend for all parameters from GPIZ2. Latent heat flux also demonstrates higher values during the La-Niña and Neutral periods, though the average TNDC is higher during the La-Niña period. The results indicate that the La-Niña period is more favorable for cyclone formation and intensification than the El-Niño and Neutral periods, as demonstrated in Table 4.

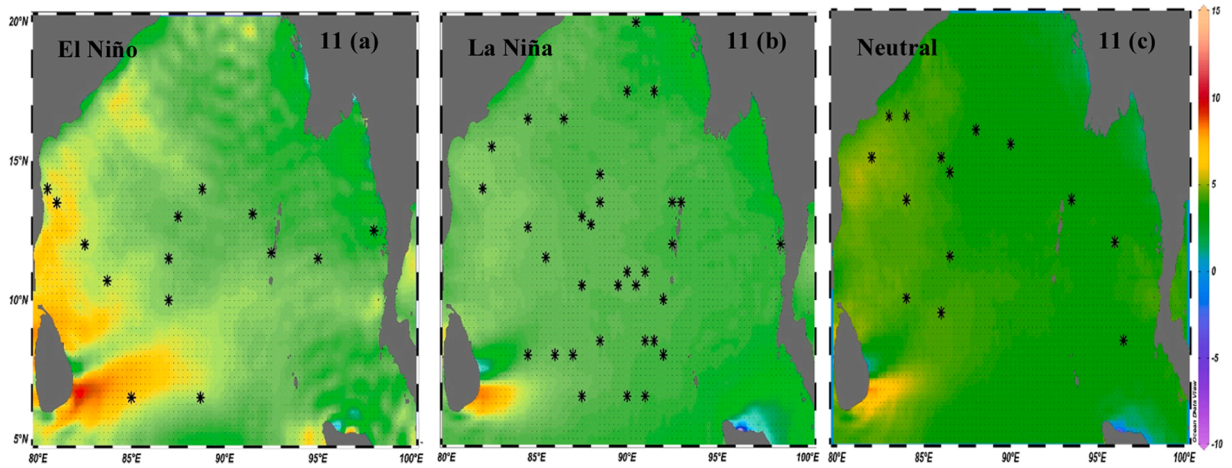

Fig. 11. (a-c): Spatial distribution of absolute vorticity at 850 hpa during post monsoon season (October-December) (a) El Niño (b) La Niña and (c) Neutral years. Black stars indicates the genesis locations.

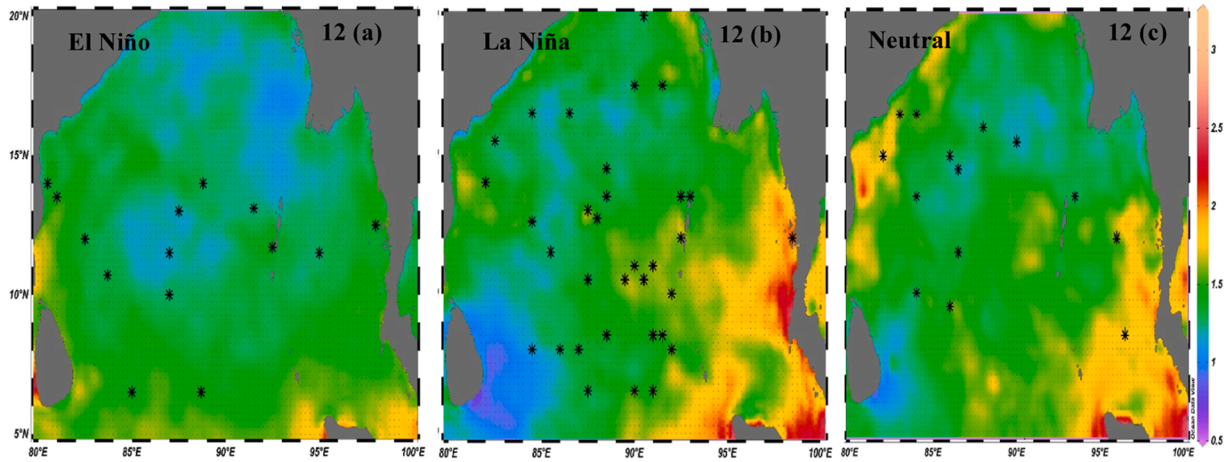

Fig. 12. (a-c): Vertical velocity at 500 hPa under (a) El Niño (b) La Niña and (c) Neutral years. Black stars indicates the genesis locations.

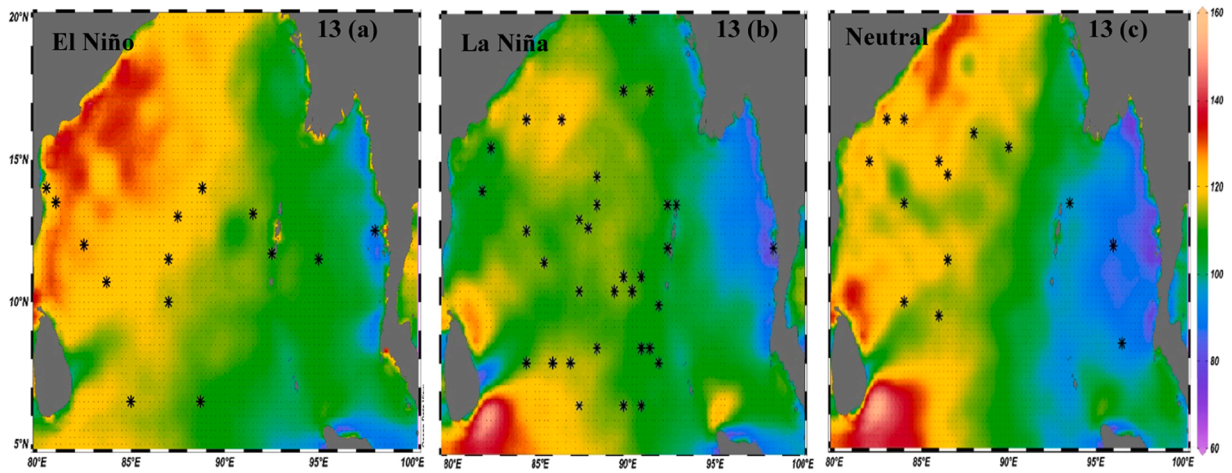

Fig. 13. (a-c): Latent Heat flux (LH) under (a) El Niño (b) La Niña and (c) Neutral years. Black stars indicates the genesis locations.

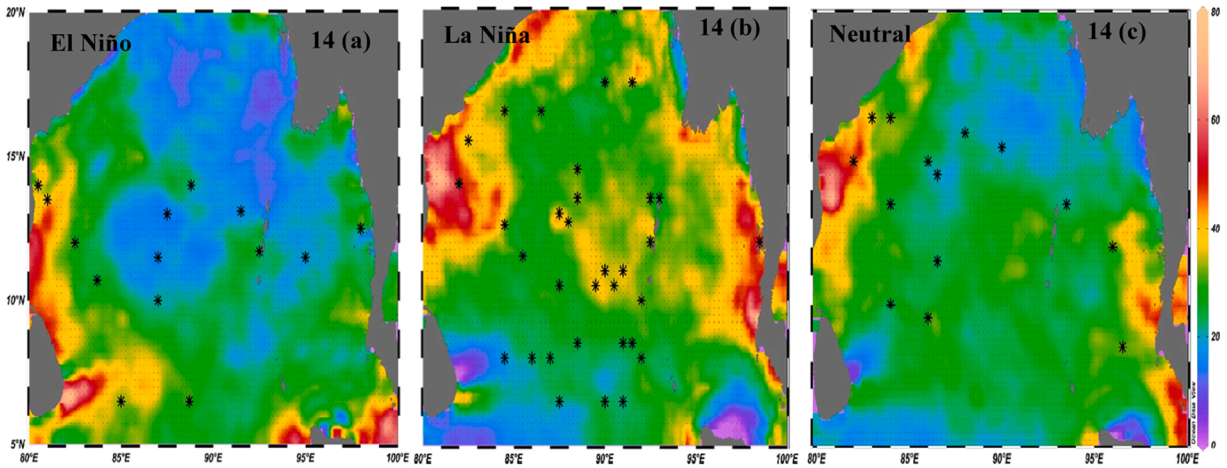

Fig. 14. (a-c): Spatial distribution of the Genesis Potential Index (GPIZ2) under **(a) El Niño, (b) La Niña, and (c) Neutral** conditions.

Table 4
Average composites of input parameters and GPIZ2 over the Bay of Bengal (BOB) during the Post-monsoon season under El-Niño, La Nina and Neutral.

Parameter	El-Niño	La-Niña	Neutral
η 850 (sec^{-1})	4.96	4.33	4.17
Ω ($pa.sec^{-1}$)	1.45	1.66	1.61
LH (w/m^2)	113.2	116.4	118.6
GPIZ2	11.3	13.1	11.7
TNDC	3.3	4.5	3.8

3.4. Relationship between the ENSO and GPIS

The GPIS calculation is based on Eq. (4), which includes ocean parameters called UOHC, SST, and D26. These parameters are analyzed for El-Niño, La-Nina, and Neutral composites. SSHA ranges from 0 to 20 cm as shown in Fig. 15 (a-c). The highest values are observed along coastal and adjacent areas of the Bay of Bengal during the La-Niña and Neutral periods, as depicted in Fig. 15 (b) and (c). According to a study by Maneesha et al. (2015) a UOHC threshold of 40 kJ/cm^2 is conducive to cyclone formation and intensification. During the study period, UOHC consistently exceeded 40 kJ/cm^2 across all three composites, ranging between 40 and 80 kJ/cm^2, with peak values occurring during the La-Niña and Neutral composites as shown in Fig. 16 (a-c). TCs predominantly

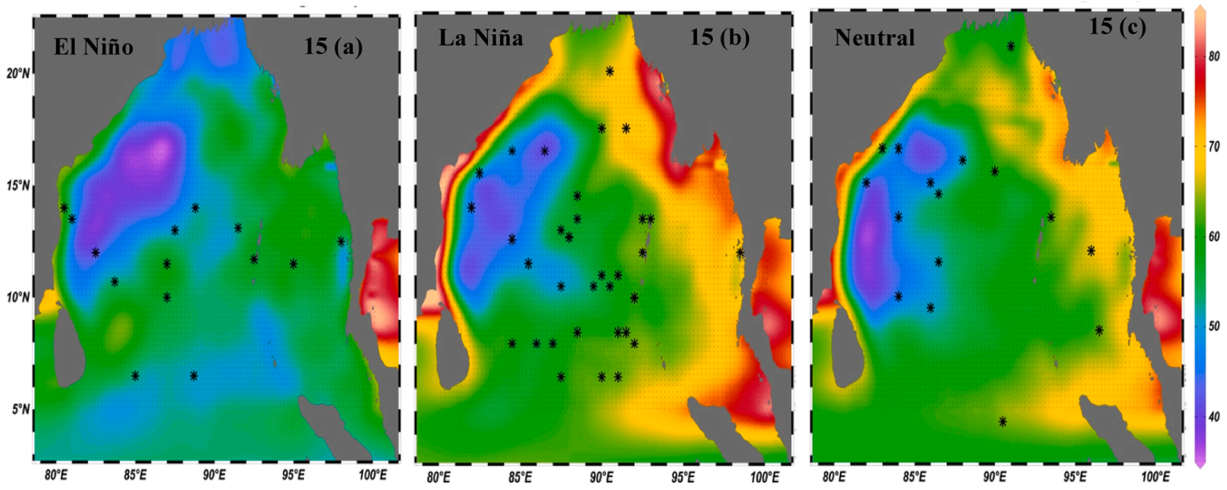

Fig. 15. (a-c): Spatial distribution of TCHP during post monsoon season from under (a) El- Nino (b) La Niña and (c) Neutral years. Black stars indicate the genesis locations.

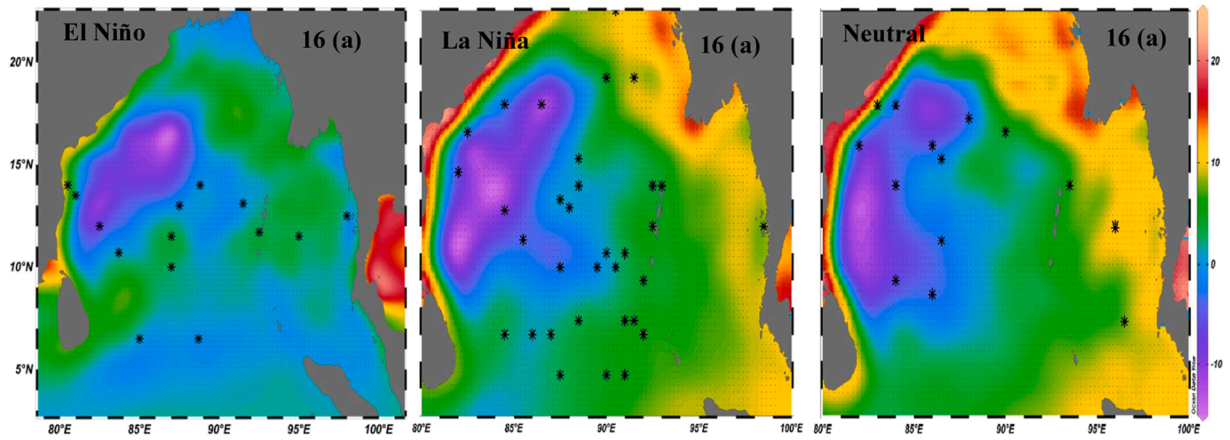

Fig. 16. (a-c): Spatial distribution of SSHA during post monsoon season from under (a) El Niño (b) La Niña and (c) Neutral years. Black stars indicate the genesis locations.

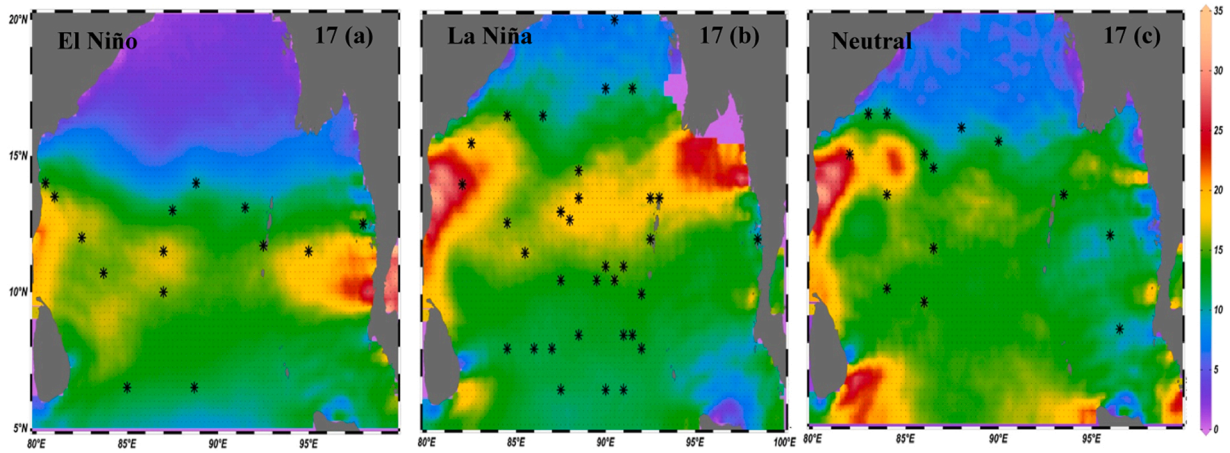

Fig. 17. (a-c): Spatial distribution of the Genesis Potential Index (GPIS) computed using oceanic parameters **(a) El Niño, (b) La Niña, and (c) Neutral** conditions.

formed over the central BoB during La-Niña compared to El-Niño and Neutral composites, as demonstrated by Fig. 16 (b). The newly developed GPIS index, which incorporates both atmospheric and oceanic parameters (such as UOHC, SSHA, and SST), exhibits values ranging from 0 to 35 $\times$ 10^{-6}. This range reflects the relative potential for cyclone genesis, with higher values indicating more favorable conditions. Fig. 17 (a-c) shows the highest values during the El-Niño period. However, tropical system genesis is lower compared to the La-Niña period, as seen in the spatial distributions in Fig. 17 (b). On average, during GPIS calculation, all parameters showed an upward trend during the La-Niña period with SST exhibiting slight changes compared to the El-Niño period. The results presented in Table 5 provide a summary of the average composite values of the input parameters. Overall, the La-Niña phase was found to be more conducive to cyclone formation during the ENSO period. Based on the GPIS results, Sea Surface Height Anomaly (SSHA) and Upper Ocean Heat Content (UOHC) emerged as two key environmental parameters influencing cyclone genesis. Although most environmental parameters (SST, D26, UOHC, SSHA) are slightly higher during La Niña years, the GPIS value is higher during El Niño years.

Table 5
Average composites of input parameters and GPIS over the Bay of Bengal (BOB) during the Post-monsoon season.

Parameter	El-Niño	La-Niña	Neutral
SSHA (m)	2.25	4.66	4.26
D_{26} (m)	68.04	71.7	70.68
SST (^{o} C)	28.57	28.77	28.5
UOHC (kJ/Cm^2)	66.6	71.5	69.3
GPIS	11.25	7.28	4.06
TNDC	3.3	4.5	3.8

This is because GPIS is a nonlinear combination of atmospheric and oceanic parameters, where certain parameter interactions enhance the index more strongly during El Niño. The difference between D26 in Tables 3 and 5 arises from the different GPI formulations (GPIZ1 vs. GPIS) and associated spatial averaging. Statistical analysis confirms that the GPIS is significantly higher during El Niño years, supporting the corrected interpretation.

3.5. *Understanding the Role of ENSO and Environmental Conditions in Genesis Potential Index*

Tan et al. (2019) exposed a comprehensive investigation into cyclone across various temporal scales to enhance our comprehension of cyclone activity within the context of climate change. Similarly, Young-Min et al., (2021) underscored the pivotal role of mean SST projections in selectively influencing different types of El-Niño events and their distant impacts on precipitation patterns. Beyond external influences from regions such as northern Australia–Indonesia and the ENSO, the Madden–Julian Oscillation (MJO) also exerts a significant influence on the genesis of cyclone in the North Indian Ocean, as highlighted by Kikuchi and Wang (2010), Yanase et al. (2012), and Krishnamohan and Mohanakumar (2012). The number of significant hurricanes may be sensitive to climate change, as indicated by previous studies (Chan, 2005; Emanuel, 2008; Zhao et al., 2011). In contrast to prior studies that primarily focused on SST dynamics, this work adopted a unique approach by considering atmospheric and oceanic parameters. This analysis explicitly targets the impacts of ENSO events and other pertinent environmental factors on the GPI. Visual examination of data illustrates a notable increase in TNDC occurrences during the La-Niña phase, as depicted in Fig. 18 (a-c). In the total year considered in this study, 38 depressions and cyclones were recorded, as indicated in Fig. 18 (b). Moreover, during the El-Niño and Neutral years, TNDC frequencies were notably lower with 17 and 15 occurrences respectively as indicated in Fig. 18 (b) and 18 (c).

During the La-Niña phase this study indicated a notable increase in relative vorticity, relative humidity, and thermal instability,

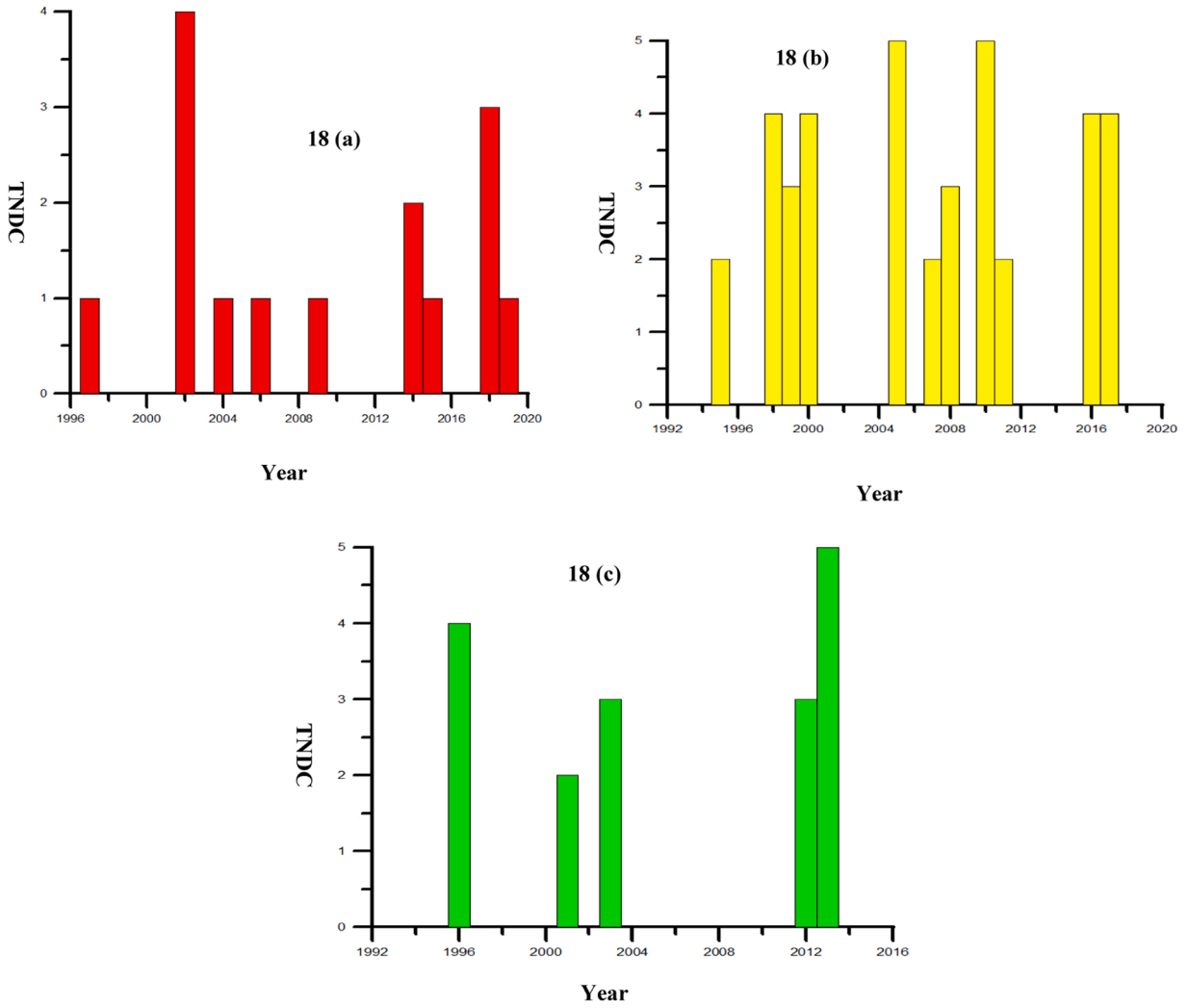

Fig. 18. (a-c): Total Number of Depressions and cyclones (TNDC) during post monsoon season under (a) El Niño (b) La Niña and (c) Neutral years.

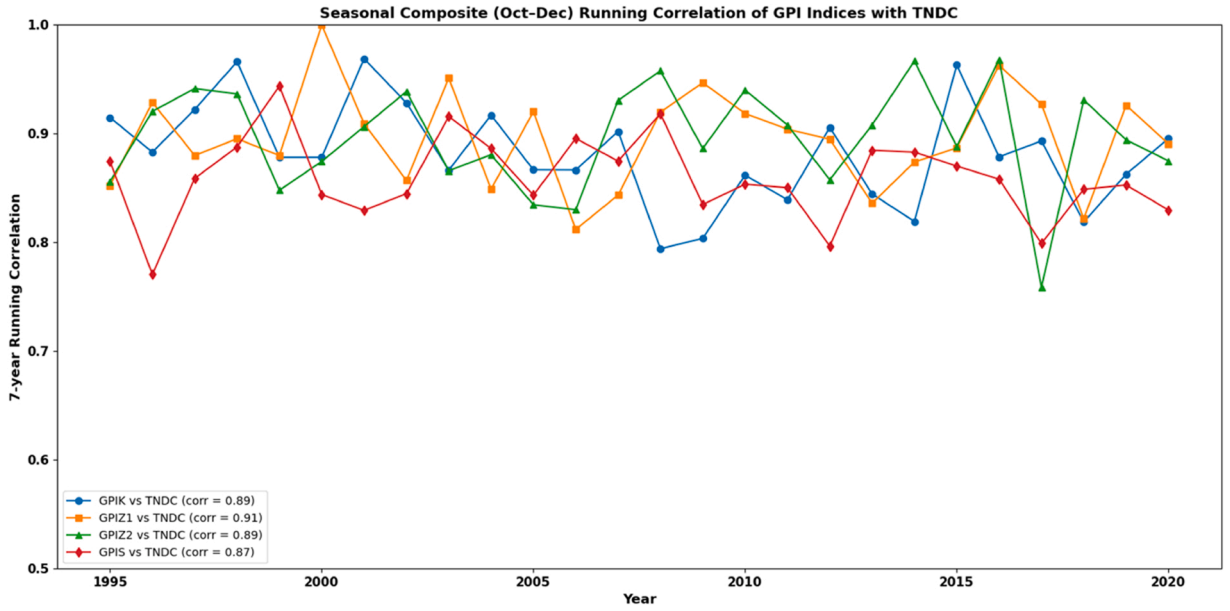

Fig. 19. 7-Year Running Correlation of GPI Indices with TNDC over the Bay of Bengal (Post- Monsoon: Oct-Dec, 1995–2019).

Table 6
Mean 7-Year Running Correlation of GPI Indices with TNDC (1995–2019, Post-Monsoon Season).

PI Index	Marker	Mean Correlation	Notes
GPIK	●	0.89	Strong positive correlation
GPIZ1	■	0.91	Slightly better representation of TNDC
GPIZ2	▲	0.89	Positive correlation with minor variability
GPIS	◆	0.87	Positive correlation; slightly lower than others

low-level vertical wind shear, absolute vorticity at 1000 hPa, SST, net long-wave radiation and D26, with D26 notably high along the Bay of Bengal coastline and elevated SST observed in the central and northern regions of the Bay of Bengal as shown in Fig. 7(b) compared to El-Niño and Neutral years. Absolute vorticity at 850 hPa, vertical velocity at 500 hPa, and latent heat fluxes, with the vertical velocity at 500 hPa, show an upward trend during La-Niña periods Fig. 13 (b). During La-Niña period LH values are higher, and most cyclone genesis occurs in the central BoB. Vital environmental indicators such as D26, SST, UOHC, SSHA and LH (from Eqs. 3 and 4) are crucial. UOHC values are higher in La-Niña and Neutral years than in El-Niño years with most cyclone genesis occurring along the BoB coast during La-Niña years. The Fig. 19 illustrates the 7-year running correlation between different Genesis Potential Indices (GPIK, GPIZ1, GPIZ2, GPIS) and the TNDC over the Bay of Bengal during the post-monsoon season (October–December) from 1995 to 2019. All indices exhibit strong positive correlations, with slight inter-annual variability. Mean correlations, shown in the legend, indicate that GPIK and GPIZ1 capture TNDC variations more effectively. The x-axis is positioned on top for clarity, with ticks evenly spaced every five years. Overall, the results highlight the robust predictive capability of these GPIs in representing seasonal cyclone activity. The Table 6 shows the mean correlations of GPIK, GPIZ1, GPIZ2, and GPIS with TNDC, highlighting strong positive relationships. GPIK and GPIZ1 exhibit slightly higher correlations, indicating better representation of seasonal cyclone variability According to previous studies higher UOHC values are favourable for the genesis of cyclone (Maneesha, 2013; Suneeta and Sadhuram, 2018). Based on the results of this study it can be emphasized that during the La-Niña phase both the atmospheric and oceanic parameters have a crucial role in the genesis and intensification of cyclones.

4. Conclusions

The current study aimed to elucidate the influence of the ENSO and other environmental conditions on GPIs in the Bay of Bengal during the post-monsoon season from 1995 to 2019. It provided detailed insights into the relationship between ENSO and various environmental factors affecting cyclone activity. These findings contribute to a deeper understanding of the factors influencing cyclone formation and intensification in the Bay of Bengal during the post-monsoon season. Using average composites from Eqs. (1−4) all GPIs exhibited higher values during the La-Niña period. Specifically, the average values were 4.16×10^{-6} for GPIK as proposed by Kotal et al. (2009) 3.5 and 13.1×10^{-2} for GPIZ1 and GPIZ2 as proposed by Zhang et al. (2016) and 7.28×10^{-6} for the GPS from Eq. 4 which incorporates UOHC, SSHA, and D26 over the period from 1995 to 2019. This observation suggests a strong association between the La-Niña phase and cyclone genesis. Most cyclonic disturbances formed during the La-Niña period, as indicated by average composites

of GPIK and GPIS. During the La-Niña phases, parameters such as relative vorticity, UOHC, and SSHA exhibited an increasing trend. This trend was also observed in other environmental elements, including net long-wave radiation, latent heat flux, D26, vertical velocity, and SST. The study found that GPIs incorporating atmospheric and oceanic parameters yielded favorable results during the La-Niña phases when compared to other phases of ENSO. Environmental variables such as relative vorticity, vertical wind shear, UOHC, SSHA, SST, latent heat, net long-wave radiation and D26 demonstrated strong associations with TCs. Vertical wind shear appeared to have more significant impact on cyclone intensity than local SST. The combined effects of vertical wind shear and SST is found to be more important than their individual contributions. This study provides an initial exploration into the relationship between GPIs and the TNDC in the Bay of Bengal during the post-monsoon season. The observed discrepancies may stem from various factors, including the unique environmental conditions in the Bay of Bengal, the influence of sub-seasonal variability, or limitations in current GPI formulations that may not fully capture all relevant dynamics. Acknowledging these complexities, future research will focus on refining these GPI calculations, incorporating additional environmental variables and investigating smaller-scale processes that could influence cyclone development. It is important to emphasize that this study is initial in terms of using the proposed GPIs and future work will build upon these findings in a phased manner to better understand the key parameters influencing TNDC. Although spatial gridded data was utilized to examine the variations, conducting partial correlation analysis presents challenges due to the limited number of ENSO events within the study period. This will also be taken in to consideration in future studies by covering longer period to include more number of cyclones. The study concludes that La-Niña periods are more conducive to cyclone formation and intensification than El-Niño and Neutral periods. The present study focuses on the genesis phase of TCs. Although La Niña composites indicate environmental conditions that could favor cyclone intensification, verifying this requires an analysis of observed maximum intensity parameters (e.g., IMD best-track data), which will be addressed in future work by integrating intensity metrics with GPI-based diagnostics. While La Niña years show a higher average number of developing cyclones (TNDC = 4.5) compared to El Niño years (TNDC = 3.3), no formal trend analysis has been conducted. Thus, this observation reflects differences between ENSO phases rather than a long-term temporal trend. Future research will explore mechanisms underlying climate change's role in distinguishing between favorable and unfavorable conditions for cyclone genesis.

CRediT authorship contribution statement

S.S.V.S Ramakrishna: Writing – review & editing, Supervision, Project administration, Data curation. **TVS Udaya Bhaskar:** Writing – review & editing, Supervision, Funding acquisition, Data curation, Conceptualization. **Ponnaganti Suneeta:** Writing – original draft, Validation, Methodology, Formal analysis, Data curation, Conceptualization.

Ethical Statement

All the authors read the manuscript, and found to have no plagiarism to the extent possible. The submitted work is original and has not been published elsewhere in any form or language. The manuscript is not submitted to any journal.

Author statement

P.Suneeta: Idea behind the work, Data collection for required work, overall work regarding this study and manuscript preparation: TVS Udaya Bhaskar: Supervised and contributed to formulating the underlying concept Improvement in writing quality: S.S.V.S Ramakrishna: Improvement in writing quality, Technical inputs in the analysis and Supervision formulation:

Funding

This study did not obtain any precise allowance from funding activities in the community, profitable, or not-for-profit sectors.

Declaration of Competing Interest

This study did not obtain any precise allowance from funding activities in the community, profitable, or not-for-profit sectors.

Acknowledgements

The authors thank the Director, INCOIS for the facilities provided to accomplish this study. The authors are thankful to all the project teams of ECMWF for providing the data sets. Thanks to IMD, New Delhi for providing the data on cyclones in the public domain. This is the INCOIS contribution number 602.

Data Availability

Data will be made available on request.

References

Ali, M., Jagadeesh, M., Lin, I.I., P, S.V., Hsu, J.Y., 2012. A neural network approach to estimate tropical cyclone heat potential in the Indian Ocean. IEEE Geosci. Remote. Sens. Lett. 9, 1114–1117.

Brian, H., Tang, Juan, Fang, Bentley, Alicia, Kilroy, Gerard, Nakano, Masuo, Myung, Sook Park, Rajasree, V.P.M., Zhuo, Wang, Allison, A.Wing, Liguang, Wu, 2020. Recent advances in research on tropical cyclogenesis. Trop. Cyclone Res. And. Rev. 9, 87–105.

Bruyere, C.L.G., Holland, J., Towler, E., 2012. Investigating the use of a genesis potential index for tropical cyclones in the North Atlantic basin. J. Of. Clim. 25, 8611–8626.

Camargo, S.J.K., Emanuel, A., Sobel, A.H., 2007. Use of a genesis potential index to diagnose ENSO effects on tropical cyclone genesis. J. Of. Clim. 20, 4819–4834.

Camargo, S.J., Sobel, A.H., 2005. Western North Pacific tropical cyclone intensity and ENSO. J. Clim. 18, 2996–3006.

Cao, X., Wang, B., Wu, Z., 2016. Intensified impact of northern tropical Atlantic SST on tropical cyclogenesis frequency over the western North Pacific after the late 1980s. Adv. Atmos. Sci. 33 (8), 919–930. https://doi.org/10.1007/s00376-016-5241-1.

Chan, J.C.L., 2005. Interannual and interdecadal variations of tropical cyclone activity over the western North Pacific. Meteor. Atmos. Phys. 89, 143–152.

Chen, H., Wu, R., Chen, Z., 2023. Impact of the winter Arctic sea ice anomaly on the following summer tropical cyclone genesis frequency over the western North Pacific. Clim. Dyn. 61 (7–8), 3971–3988. https://doi.org/10.1007/s00382-023-06789-5.

Chia, Hsin Hsing, Ropelewski, C.F., 2002. The interannual variability in the genesis location of tropical cyclones in the Northwest Pacific. J. Of. Clim. 15, 2934–2944.

DeMaria, M., Knaff, John A., Connell, Bernadette H., 2001. A tropical cyclone genesis parameter for the tropical Atlantic. Weather Forecast. (16), 219–233.

Du, Y., Xie, S.-P., Huang, G., Hu, K., 2011. Tropical Indian Ocean influence on Northwest Pacific tropical cyclones in summer following strong El Niño. J. Clim. 24 (1), 315–322. https://doi.org/10.1175/2010JCLI3890.1.

Emanuel, K.A., 2008. The hurricane-climate connection. B. Am. Meteorol. Soc. 89, ES10–ES20.

Emanuel, K.A., Noolan, D., 2004. Tropical cyclone activity and global climate system, preprints. 26th conference on hurricanes and tropical Meteorology Miami Fla. Am. Met. Soc. 240–241.

Felton, Clifford, S., Subrahmanyam, Bulusu, Murty, V.S.N., 2013. ENSO modulated cyclogenesis over the Bay of Bengal. J. Clim. 26, 9806–9818.

Girishkumar, M.S., Ravichandran, M., 2012. The influences of ENSO on tropical cyclone activity in the Bay of Bengal during October-December. C02033 J. Geophys. Res. 117. https://doi.org/10.1029/2011JC007417.

Goswami, B.N., Ajayamohan, R.S., Xavier, P.K., Sengupta, D., 2003. Clustering of synoptic activity by Indian summer monsoon intraseasonal oscillations. Geophys. Res. Lett. 30, 1431. https://doi.org/10.1029/2002GL016734.

Harla, K.K., Aldrian, E., An, S.I., Cavalcanti, I.F.A., de Castro, M., Zou, L., 2013. Climate phenomena and their relevance for future regional climate change. In Climate change 2013 the physical science basis: Working group I contribution to the fifth assessment report of the intergovernmental panel on climate change. Cambridge University Press, pp. 1217–1308.

Hu, F., Li, T., Liu, J., Bi, M., Peng, M., 2018. Decrease of tropical cyclone genesis frequency in the western North Pacific since 1960s. Dyn. Atmos. Oceans 81, 42–50.

Huang, L., Zhang, W., Chen, L., 2024. Impact of the winter regional Hadley circulation over the western Pacific on the frequency of following summer tropical cyclone landfalling in China. J. Clim. 37 (13), 3521–3541. https://doi.org/10.1175/JCLI-D-23-0542.1.

Kikuchi, K., Wang, B., 2010. Formation of tropical cyclones in the northern Indian Ocean associated with two types of tropical intraseasonal oscillation modes. J. Meteor. Soc. 88, 475–496.

Kotal, S., D., Kundu, P., K., Roy Bhowmik, S., K., 2009. Analysis of cyclogenesis parameter for developing and non-developing low pressure systems over the India Sea. Nat. Hazards 50, 389–402.

Krishnamohan, K.S., Mohanakumar, K., 2012. The influence of Madden–Julian oscillation in the genesis of north Indian Ocean tropical cyclones. Theor. Appl. Climatol. (109), 271–282.

Li, Z., Yu, W., Li, T., Murty, V., S., N., Tangang, F., 2013. Bimodal character of cyclone climatology in the Bay of Bengal modulated by monsoon seasonal cycle. J. Clim. 26, 1033–1046.

Lin, I., I., Chan, J., C., L., 2015. Recent decrease in typhoon destructive potential and global warming implications. Nat. Commun. 6, 7182.

Lin, X., Wang, L., Gao, J., Chen, X., Zhang, W., 2021. Intraseasonal variability of the East Asia-Pacific teleconnection and its impacts on multiple tropical cyclone genesis over the Western North Pacific. Front. Earth. Sci. 8, 1–17.

Liu, K., S., Chan, J., C., L., 2013. Inactive period of western North Pacific tropical cyclone activity in 1998-2011. J. Clim. 26, 2614–2630.

Mahala, B., K., Nayak, B., K., Mohanty, P., K., 2015. Impacts of ENSO and IOD on tropical cyclone activity in the Bay of Bengal. Nat. Hazards 75, 1105–1125.

Maneesha, K., 2013. Role of Upper Ocean in the intensification and movement of tropical cyclones and their associated biogeochemical response in the Bay of Bengal Ph.D Thesis. Andhra University, Visakhapatnam India, p. 238.

Maneesha, K., Sadhuram, Y., Prasad, K., V., S., R., 2015. Role of upper ocean parameters in the genesis intensification and tracks of cyclones over Bay of Bengal. J. Oper. Oceanogr. 8 (2), 133–146.

Michiaki Yumoto, K. Kita, Y. N. Chen, T. Saito, T. Kakinami, M. Shinohara, Y. Otani. 2001. Western North Pacific tropical cyclones and ENSO in NIED CGCM. Report of the National Research Institute for Earth Science and Disaster Prevention (61), 14.

Mishra, Siba Prasad, Sethi, Kumar Charan, Mishra, Durga Prasad, Siddique, Mohammed, 2019. Pre-monsoon cyclogenesis over Bay of Bengal. Int. J. Recent. Technol. And. Eng. (IJRTE) 8, 4895–4908.

Roy Bhowmik, S., K., 2003. An evolution of cyclone genesis parameter over Bay of Bengal using model analysis. Mausam 54, 351–358.

Royer, J., F., F., Chauvin, B., Timbal, P., Araspin, Grimal, D., 1998. A GCM study of the impact of greenhouse gas increase on the frequency of occurrence of tropical cyclones. J. Of. Clim. 38, 307–343.

Sadhuram, Y., Maneesha, K., Ramana Murty, T., V., 2012. Intensification of Aila (May 2009) due to a warm core eddy in the North Bay of Bengal. Nat. Hazards 63, 1515–1525.

Sadhuram, Y., Murty, T., V., R., Somayajulu, Y., K., 2006. Estimation of tropical cyclone heat potential in the Bay of Bengal and its role in the genesis and intensification of storms. Indian. J. Mar. Sci. 35 (2), 132–138.

Sadhuram, Y., Rao, B., P., Sastry, P., N., M., Subrahmanyam, M.,V., 2004. Seasonal variability of Cyclone Heat Potential in the Bay of Bengal. Nat. Hazards 32, 191–209.

Singh, O., P., Khan, T., M., A., Rahman, M., S., 2000. Changes in the frequency of tropical cyclones over the North Indian Ocean. Meteor. Atmos. Phys. 75, 11–20.

Suneeta, P., Ramakrishna, S.S.V.S., 2021. Modified tropical cyclone genesis potential index over the Bay of Bengal during southwest and post-monsoon seasons. J. Earth Syst. Sci. 130, 196.

Suneeta, P., Sadhuram, Y., 2018. Tropical cyclone genesis potential index for Bay of Bengal during peak post-monsoon (October-November) season including atmosphere-ocean parameters. Mar. Geod. 41 (1), 86–97.

Ta-Huu, Chinh, Sato, Tomonori, 2018. Effect of ENSO phase on the contribution of environmental variables to tropical cyclone genesis in the western North Pacific. Int. J. Clim. 1–13.

Tan, K., Huang, P., Liu, F., Murakami, H., Hsu, P., C., 2019. Simulated ENSO's impact on tropical cyclone genesis over the western North Pacific in CMIP5 models and its changes under global warming. Int. J. Clim. 39, 3668–3678.

Tippet, M., K., Camargo, S., J., Sobel, A., H., 2011. A Poisson regression index for tropical cyclone genesis index and the role of large scale vorticity in genesis. J. Of. Clim. 24, 2335–2357.

Vissa, N., K., Satyanarayana, A., N., V., Kumar, B., P., 2013. Intensity of tropical cyclones during pre and post monsoon seasons in relation to accumulated tropical cyclone heat potential over Bay of Bengal. Nat. Hazards 68 (2), 351–371.

Wada, A., Usui, N., 2007. Importance of tropical cyclone heat potential for tropical cyclone intensity and intensification in the Western North Pacific. J. Oceano 63, 427–447.

Wu, M., Chang, W., Leung, W., 2004. Impacts of El-Niño-Southern Oscillation events on tropical cyclone land falling activity in the western North Pacific. J. Clim. 17, 1419–1428.

Xu, Kang, Tam, Chi-Yung, Liu, Boqi, Chen, Sheng, Yang, Xiaoyi, He, Zhuoqi, Xie, Qiang, Wang, Weiqiang, 2020. Attenuation of Central Pacific El Niño Amplitude by North Pacific Sea Surface Temperature Anomalies. J. Of. Clim. 33, 6673–6688.

Yanase, W., Satoh, M., Taniguchi, H., Fujinami, H., 2012. Seasonal and intraseasonal modulation of tropical cyclogenesis environment over the Bay of Bengal during the extended summer monsoon. J. Clim. 25, 2914–2930.

Yaukey, H. Peter, 2014. Intensification and rapid intensification of North Atlantic tropical cyclones: geography, time of year, age since genesis, and storm characteristics. Int. J. Climatol. (34), 219–233.

Young-Min, Yang, Jae-Heung, Park, Soon-II An, Bin, Wang, Xiao, Luo, 2021. Mean sea surface temperature changes influence ENSO-related precipitation changes in the mid-latitudes. Nat. Commun. https://doi.org/10.1038/s41467-021-21787-z,12(1).

Zhang, M., Zhou, L., Chen, D., Wang, C., 2016. A genesis potential index for Western North Pacific tropical cyclones by using ocean parameters. J. Geophys. Res. Oceans 121, 7176–7191.

Zhao, H., Wu, L., Zhou, W., 2011. Interannual changes of tropical cyclone intensity in the western north Pacific. J. Meteor. Soc. Jpn. 89, 243–253.